How a Turbocharger Works

The turbocharger has been a great source of maximizing efficiency of an internal combustion engine since the late 1920's. Alfred Buchi was the engineer that came up with the idea to utilize the wasted energy that is expelled through the exhaust system. It was in 1915 that he created his first prototype, which failed. This however did not stop the persistent inventor. He worked on it for another 10 years before he produced the first practical, functioning turbocharger that increase efficiency of an engine by 40%.

Courtesy of www.turbododge.com

Over the years however, the turbocharger has benefitted the internal combustion engine much more than maximizing its efficiency. It has been utilized to create massive gains in power output of an engine compared to the amount of power achievable with a naturally aspirated platform (no forced induction utilized). Turbocharges, utilized in the right way, can increase a non-turbocharged motor from 200bhp to over a 1000bhp; with supporting modifications.

Courtesy of John Hoet

How It Works

A turbocharger is composed of 3 basic parts, a **compressor**, a **turbine**, and a **center housing**. The turbine is the section of the turbocharger where the exhaust gases of the engine are forced through to cause the turbine wheel to spin. This rotation energy is then transferred through the center housing and into the compressor by means of a **stainless steel**, or sometimes **inconel**, shaft. This center housing is comprised of **journal** or **ball** bearings, depending upon the application, as well as oil lubrication ports and drains. This allows the bearings to well lubricated, as well as cooled, to handle the immense rotational speeds and heat that they have to endure. Some center housings have integrated coolant passages to provide supplemental cooling. This is not always required, but it does drastically improve a turbochargers life, as well as protect it in circumstances where it is put under high or prolonged demand. The compressor does exactly what it's named for, it compresses air.

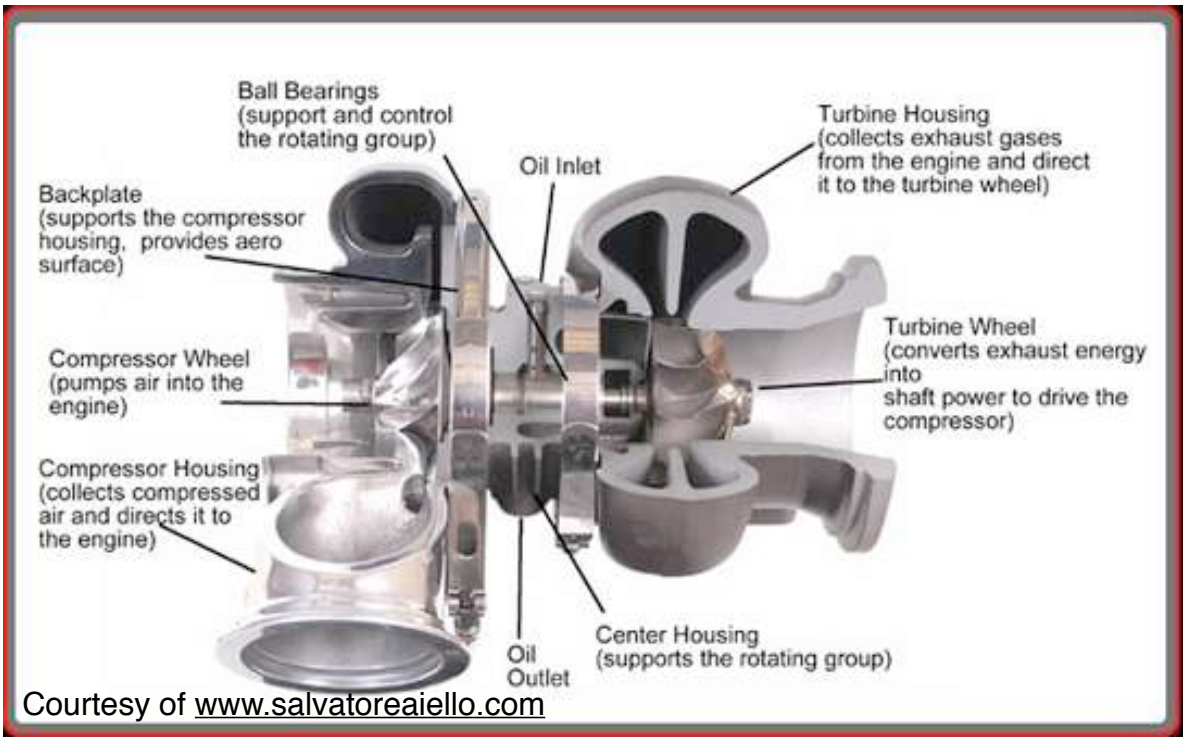

The compressor is spun by the rotational force created by exhaust gases flowing through the turbine. This would feed the intake side of the motor. Air is inducted into the compressor and then compressed into the piping, feeding the air intake ports of the motor. This creates an increased flow, as well as density, of air to be fed into the combustion chambers of the motor.

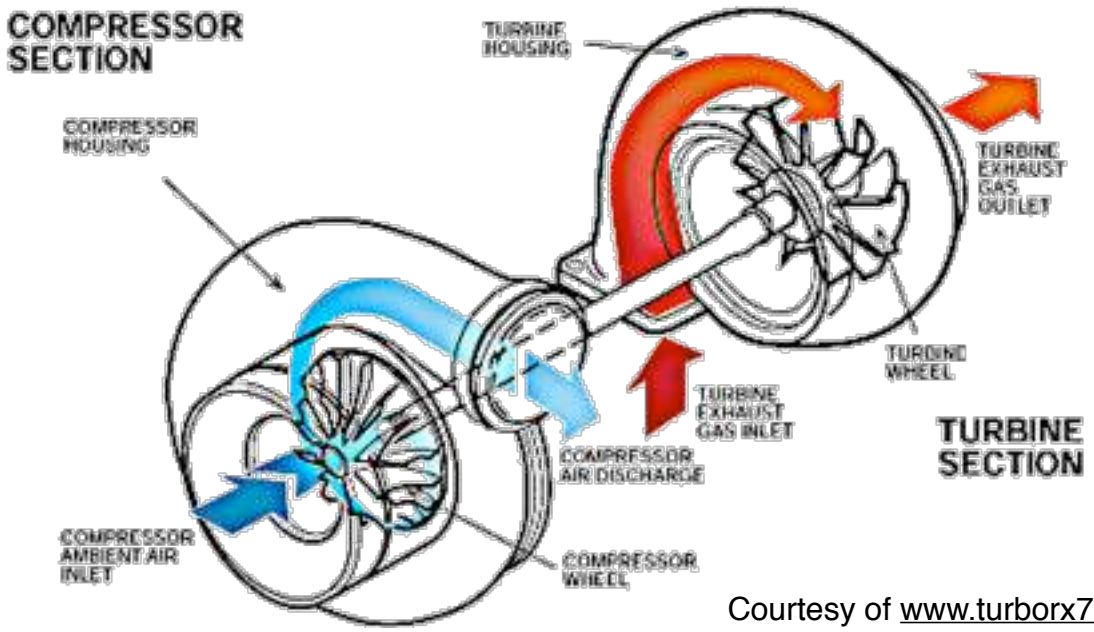

Courtesy of www.turborx7.com

So quite simply, the more oxygen that can be forced into the motor means that more fuel can be added to maintain a stabilized combustion. This in turn causes a larger, more powerful combustion. Thus, increasing the power output of the motor.

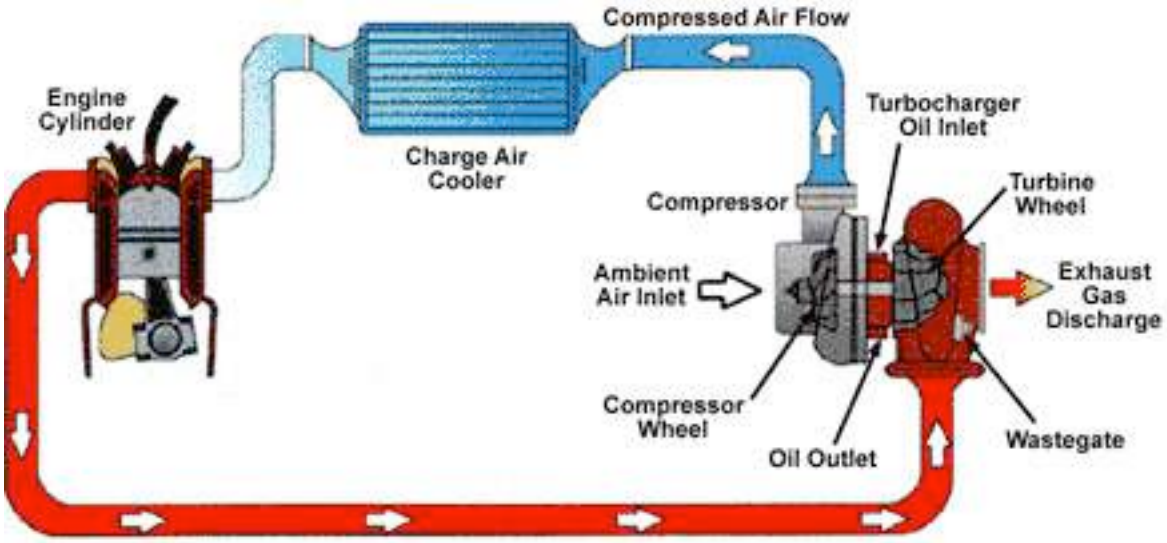

Courtesy of www.areadiesel.com

The diagram above depicts the process of utilizing the engines exhaust gases to force clean air into the motor for combustion. In the diagram above, you may notice a "**charge air cooler**" or more commonly known as an **intercooler**. Although not utilized in all cases, most turbocharged platforms utilize an intercooler to cool the compressed air back down to the ambient air temperature. This is due to the fact that heat is transferred from the turbine of the turbocharger to the compressor by

consequence of the exhaust gases flowing through it. This causes an undesired effect of heating the compressed air that is formed by the compressor of the turbocharger. A higher temperature air becomes less dense of oxygen molecules, which intern cause less oxygen to flow into the combustion chambers and produces a smaller, less powerful combustion (less power output). **So to counter this effect**, an intercooler is implemented to cool the air back down.

Courtesy of John Hoet

Hopefully, this has helped you to understand the dynamics and purpose of a turbocharger. The turbocharger seems like a simple aspect, but it can get very in-depth and specific to select the correct one for an application. They are highly engineered to exact tolerances and flow patterns, and they are very easy to destroy if you do not understand their limitations.

Noise of Turbocharger Compressors

Hua Chen

Noise of Turbocharger Compressors

Hua Chen
Marine Engineering College, Dalian Maritime University
1 Linghai Road, Dalian, China 116026
huachen204887@163.com

ABSTRACT

Noise produced by turbocharger compressors is becoming a major concern of turbocharging industry. But confusion exists regarding the sources of the noise. This paper discusses this noise from an aerodynamicist's point of view. Blade passing frequency noise and flow instability related noise are in particularly examined. Focus is on how these two noises are generated and how they may be controlled at source level. The aerodynamic causes of the noises are described and identified, and measures to reduce them at compressor design stage are proposed.

KEYWORDS

noise, turbocharger, compressor, instability

NOMENCLATURE

A	Flow passage area (m^2)
B	Blade number
BPF	Blade passing frequency (Hz)
F	Force (N)
f	Frequency (Hz)
f*	dimensionless frequency = f /rps of rotor
h	Specific enthalpy (J/kg)
L	A characteristic length of impeller, eq. (1)
LE	Leading edge
m	Circumferential wave number
$\dot{m}$	Mass flow rate (kg/s)
P	Pressure (N/m^2)
P.S.	Pressure side
RI	Rotating instability
r	Radius (m)
rps	Revolution per second (1/s)
SPL	Sound pressure level (dB)
S.S.	Suction side
T	Time period of vortex shedding (s)
TLV	(LE) Tip leakage vortex
U	Impeller blade peripheral (tip) speed (m/s)
URANS	Unsteady Reynolds averaged Navier-Stoke eqs.
V	Absolute velocity (m/s)

Greek Symbols

β	Angle of relative velocity, measured from meridional direction (rad.)
δ_0	Half of the shear layer thickness, see Fig. 9(a)
ρ	Density (kg/m^3)
τ	Torque (N-m)
Ω	Angular speed of rotor (rad./s), rotor rps (1/s)
Φ, φ	Flow coefficient based on impeller outlet blade speed

Subscript

0	Stagnation or total state
1	Impeller inlet
2	Impeller exit
R	Rotation
r	Radial direction
RI	Rotational instability
u	Tangential direction
z	Axial direction

Superscripts

~	Root square mean

1. INTRODUCTION

Noise produced by turbochargers is a concern for their users. With higher charging pressures for downsized internal combustion engines, the noise is becoming louder and there is a growing demand to control it. Compared with other aspects of turbochargers and with aero engines, the noise of turbochargers draws little attention until recently. Feld et al. (**1**) described the design and set up of an acoustic test facility for large turbocharger compressors for marine applications. Influences of inlet distortion and vaned diffuser to blade passing frequency (BPF) noise were studied. Clay and Moch (**2**) reported the development of an acoustic test chamber for small turbochargers. Rämmal and Åbom (**3**) discussed sound generating mechanisms of turbocharger compressors and described a model for evaluating the passive acoustic effect of turbocharger turbines to engine exhaust pulses. Brand et al. (**4**) presented their work of acoustic decouplings to against turbocharger noise being transferred to engine exhaust system. Schweizer and Sievert (**5**) examined the noise generated by rotor-bearing-shaft system. Tanna et al (**6**) portrayed their work on reducing the BPF noise of turbocharger compressors employing a ported shroud. Lee et al (**7**) conducted an experimental study of the noise radiated by a turbocharger. A turbocharger test rig was mounted on an anechoic chamber, and noise was measured with a free field microphone placed at 0.8 m from the inlet of the compressor. A narrow band noise was found at a frequency about 3 times of rotor rev. and was the dominant frequency in most config-

urations. This was attributed to the experimental setup. Sheng (**8**) gave a presentation on turbocharger noises identifying a number of them. Kabral et al. (**9**) proposed an acoustic method for investigating turbocharger flow instability in which acoustic features of the sound generation and scatting by the compressor near surge were investigated. The results show that broadband noise at near surge condition is considerably higher than at other conditions, and a notable hump centred at 45% shaft speed was found and considered to be rotating stall related. Karim et al. (**10**) presented their study of 'hiss/whoosh' or broad noise of a turbocharger compressor at off-design conditions, and identified the best configuration of inlet guide vanes and grooves/steps in front of the impeller. Dehner R et al. (**11**) tested a turbocharger compressor for instability at the low-flow range using acoustic signals. They recognized the link between surges and incidence angle at impeller inlet and others. Surge noise identification and control was discussed by Kuang X. et al. (**12**). Åbom and Rämmal (**13**) reported their development of a compact silencer for noise at KHz range. Broatch et al. (**14**) carried out experimental and computational studies of the broad band noise of a turbocharger compressor at a peak pressure ratio of 2.24:1. Biet and Baar (**15**) described an acoustic climate camber for acoustic measurement of turbochargers at cold environmental conditions. Gupta et al. (**16**) investigated the methods to reduce turbocharger whistle noise transmitted into passenger cabin. Identification of the noise sources, aero or mechanical, was mentioned. Galindo et al. (**17**) studied the effects of real running shroud clearance of a small turbocharger compressor on its acoustic behavior in near surge condition, taking into account the effects of rotation, thermal expansion and shaft motion. No significant changes in the behavior were found. It was suggested that in this working condition, the tip clearance is immersed in a region of strongly swirling flow, therefore cannot establish any coherent noise source mechanism.

Majority of the noise generated by turbochargers are flow related. This asks for a good understanding of the fluid dynamics side of this type of noise, which is currently unsatisfactory. Often the source of a noise is misidentified, or simply described with general term of 'instability' or 'rotating stall'. Of the turbine and compressor in a turbocharger, more noises are generated and transmitted by the compressor. Because of the flow acceleration nature of the turbine, thicker and heavier turbine casing, and the relatively good damping characteristics by modern mufflers and after-treatment devices, turbine noise is less of a concern. The compressor on the other hand is a flow diffusion device and subject to flow instability. The instability generates noise. For these reasons, this paper discusses compressor noise from aerodynamic point of view. The focus will be the underline mechanism of the noise, that is, how various noises are generated by the compressor. The measures to control these noises will also be addressed.

2. BLADE PASSING FREQUENCY (BPF) NOISE

This noise is mainly caused by blade loading. The noise caused by blade thickness should be small and will not be discussed here. The pressure difference (loading) on the two surfaces of a blade generates a pressure disturbance when the blade rotates. This disturbance propagates as sound wave, its frequency is equal to blade number x blade rotating frequency, and its amplitude increases with the pressure difference. **Figures 1** and **2** show the measured compressor operating condition and casing blade loading of a 400mm, 30° backsweep centrifugal impeller operated at a subsonic tip Mach number of 0.6. The blade loading (and the BPF noise) reduces and shifts toward impeller LE with compressor mass flow, from operating points (A) to (D). When flow instability occurs, operating point (G), the loading, particularly the front part, greatly reduces. The change of the loading with mass flow is related to the change of incidence angle to the blade.

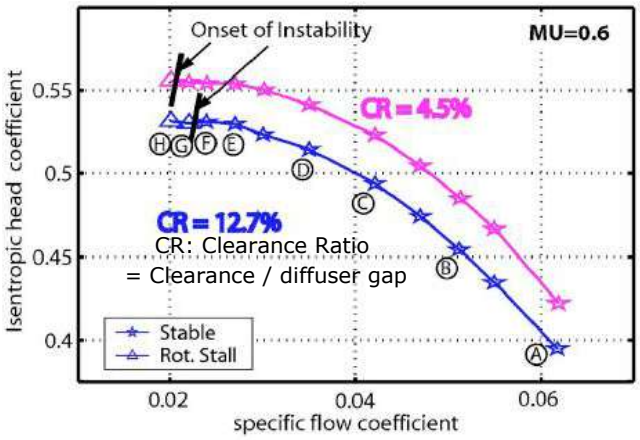

Fig. 1 Head coefficients of a centrifugal compressor with two shroud clearances. (18)

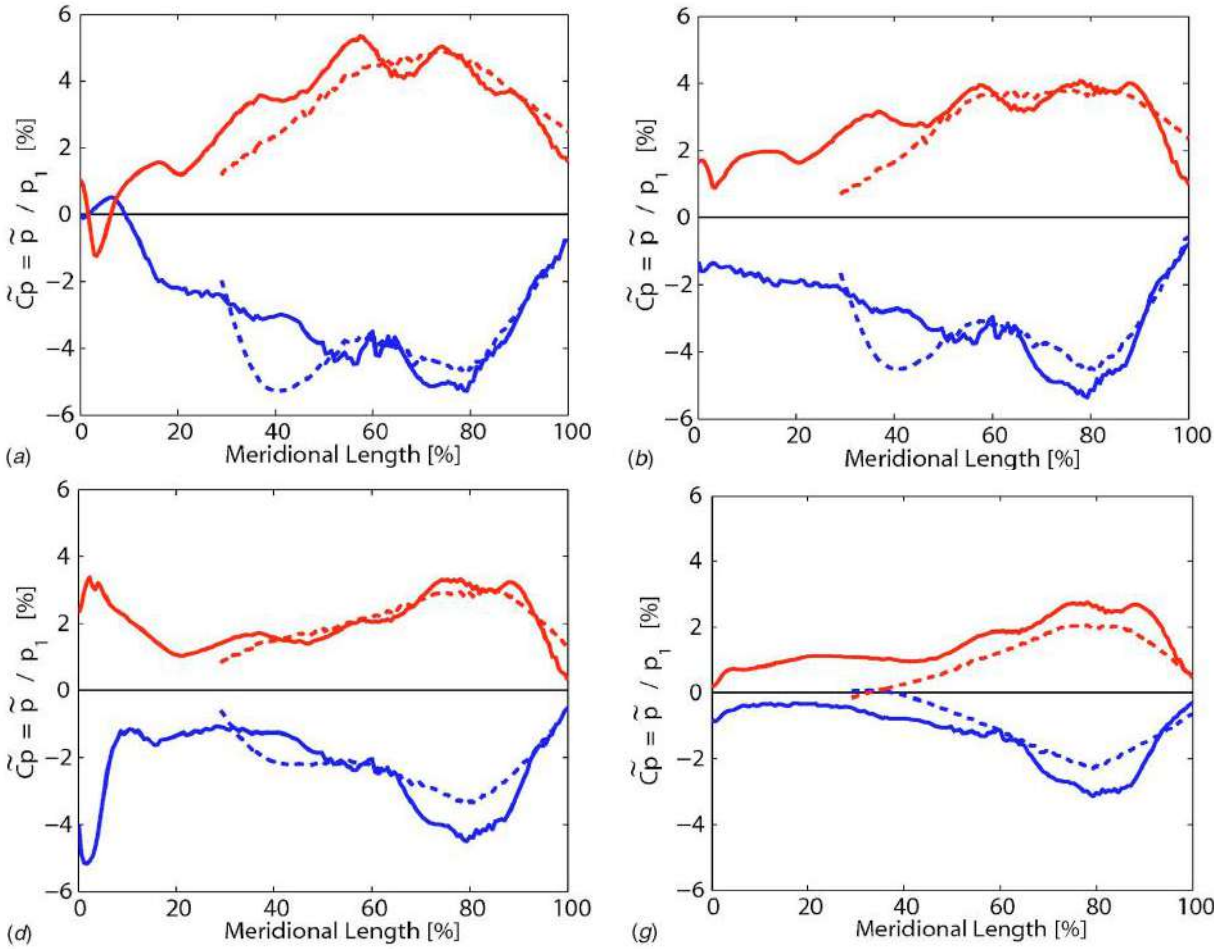

Fig. 2 Casing measurement deducted blade loading at operating points (A), (B), (D) and (G) of Fig. 1 Clearance ratio CR = 12.7%, solid and broken lines for full and splitter blades respectively. (18)

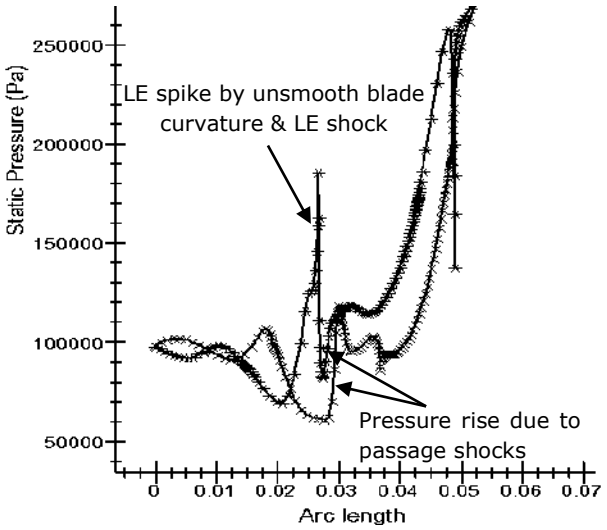

Fig. 3 Shroud pressure loading of a turbocharger compressor at 547m/s tip speed & peak efficiency point by CFD

Figures 3 gives the calculated blade loading of a small turbocharger compressor working at supersonic flow condition. A striking feature of it is the sharp pressure spike at the LE. This is due to LE bow shock and the discontinuity of the blade surface curvature in the LE region. The LE shock is responsible for the 'buzz-saw' type noise commonly detected in front of transonic compressors and fans (**19**). The shock strength may be reduced by using a sharp and thin LE. The LE spike can also be reduced by using curvature smooth blades (**20**). Both LE spike and passage shocks can cause flow to separate, the link between flow separation and noise will be discussed later.

Figure 4 presents calculated static pressure distribution at inlet duct of a small turbocharger compressor. The impeller has six main and six splitter blades. Twelve circumferential waves are visible, and the influence of the sixth harmonic of rotating frequency is cut-off rapidly.

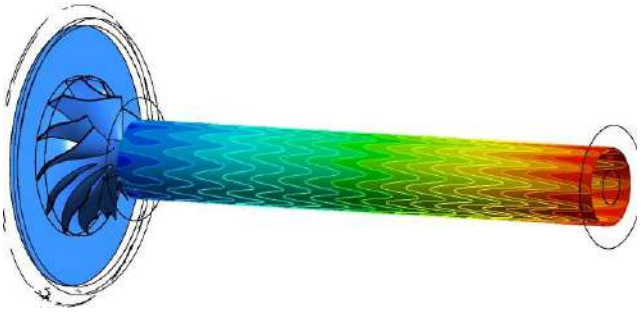

Fig. 4 Instantaneous pressure wave pattern by URANS at inlet duct of a 6+6 bladed turbocharger compressor operating at inducer tip speed of 401.5m/s and near choke

Figure 5 gives calculated SPL at the compressor inlet and outlet. The inlet is dominated by high order harmonics of full blade passing (6 x rotating speed), particularly even number modes 2, 4 and 6. The outlet on the other hand is dominated by the fundamental mode of full blade passing. According to the flow field measurement by Roduner et al. (**21**), the high order harmonics are damped by vaneless diffuser.

URANS is not the most accurate CFD method for sound source calculation. More sophisticated methods such as Large Eddy Simulation (LES) and Detached Eddy Simulations (DES) are more accurate but require more computational power. CFD is usually used only in source computing, sound transmission can be calculated by simpler methods.

The overall blade force is connected directly with compressor power. Using the Euler's turbomachinery eq., the power of a compressor is

$$\tau\Omega = \dot{m}(h_{02}-h_{01}) = \dot{m}\left(U_2V_{u2}-U_1V_{u1}\right) = \dot{m}U_2V_{u2}$$

$$\tau\Omega = \rho_1 A_1 V_{z1}\left(1+\frac{V_{r2}}{U_2}\tan\beta_2\right)U_2{}^2$$

The total blade force F and the force on single blade F/B, where B is blade number, are

$$F = \tau / L = \tau\Omega/(\Omega L) \approx \rho_1 A_1 \frac{V_{z1}}{U_2}\left(1+\frac{V_{r2}}{U_2}\tan\beta_2\right)U_2{}^2$$

$$F/B \approx \rho_1 A_1 \frac{V_{z1}}{U_2}\left(1+\frac{V_{r2}}{U_2}\tan\beta_2\right)U_2{}^2/B \qquad (1)$$

Where L is a characteristic length, and may be approximated by the impeller tip radius. So, the force creating the BPF noise increases with compressor size A_1, compressor inlet flow coefficient V_{z1}/U_2 and blade tip speed U_2. U_2 also links to the BPF, so depending on where the BPF is on the sensitivity curves of the human ears, changes in U_2 may have different effects on human perception to the BPF noise. $V_{r2}/U_2 > 0$ is impeller exit flow coefficient. β_2 is the impeller exit flow angle and is approximately equal to impeller exit blade angle, commonly referred to as backsweep angle since $\beta_2 < 0$ in turbocharger compressors. An increase of the backsweep angle (β_2 becomes more negative) reduces blade loading, particularly at high flows, see **Figure 6**, hence decreases BPF noise. Large backsweep angle also increases the stagger of the blades, resulting in higher blocking by the blades to sound propagation downstream.

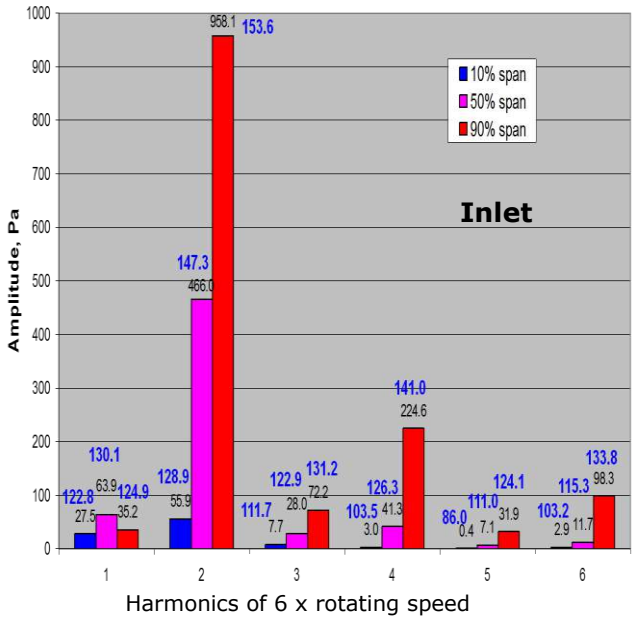

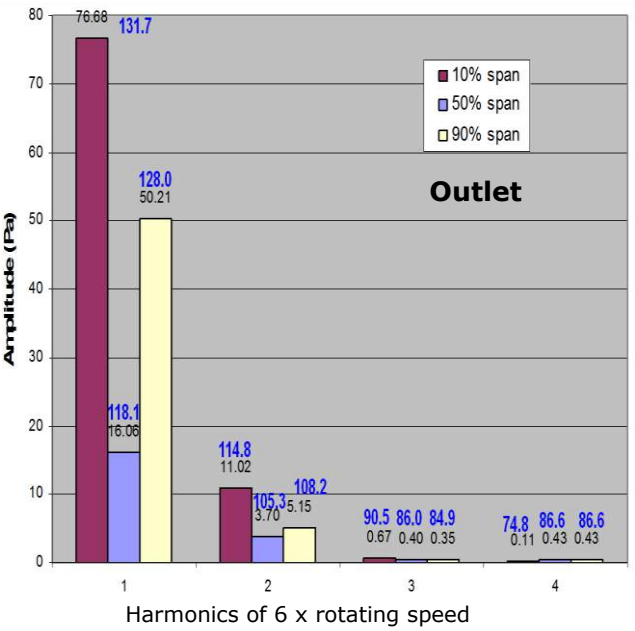

Fig. 5 Calculated pressure wave amplitude and SPL dB (in blue) at inlet and outlet of the compressor in Fig. 4

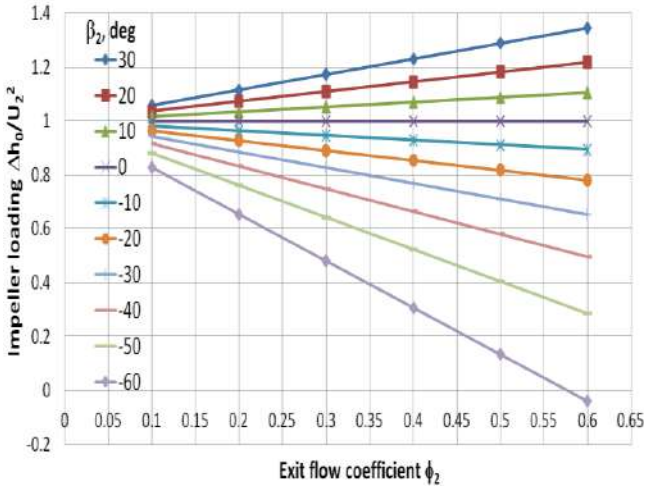

Fig. 6 Effects of impeller blade exit angle and exit flow coefficient on stage loading coefficient

Blade number is very important to the efficiency and BPF noise of small turbocharger compressors. Viscous friction loss is high in such compressors, and reducing the blade number often brings efficiency benefit. This, however, needs to be balanced with BPF noise consideration. F/B, the force per blade, increases with reduction of blade number B. Use of full bladed impellers is an effective way to reduce BPF noise and solve this conflict. Not only the single inducer blade loading is reduced and BPF moves up to the less sensitive range of human ears, but also the damping to the BPF noise is increased, because the damping is proportional to e^{-Bx} below sound wave cut-off. **Figure 7** demonstrates these effects. In compressor design stage, more blades may be achieved with shorter blades to maintain blade 'picth-chord' ratio so that aero performance would not be affected. Mechanical properties and manufacturing capability of the impeller may also be kept.

3. NOISE DUE TO FLOW INSTABILITY

A turbocharger compressor usually composes of three components: a centrifugal impeller, a diffuser and a volute housing. The impeller and the diffuser decelerate flow and are subject to certain diffusion limits before the flows separate. The volute housing can both decelerate and accelerate flow depending on its mass flow rate: if the rate is higher than the one it was designed for, the flow will accelerate in it; if the rate is lower than the design value, the flow will diffuse in it and may eventually stall. Flow separations are unsteady and companied with vortices generation. Often strong tonal and broadband noises are reported when a compressor is closed to surge. At this condition, the compressor as a flow diffusion device is working at its maximum capacity. They are several noise generating mechanisms by flow instability inside compressors, and they are discussed here. We restrict ourselves to the open shroud impellers with shroud clearance and vaneless diffusers. **Figure 8** shows different compressor instabilities on the map of such a compressor and the associated casing pressure signals taken close to impeller LE.

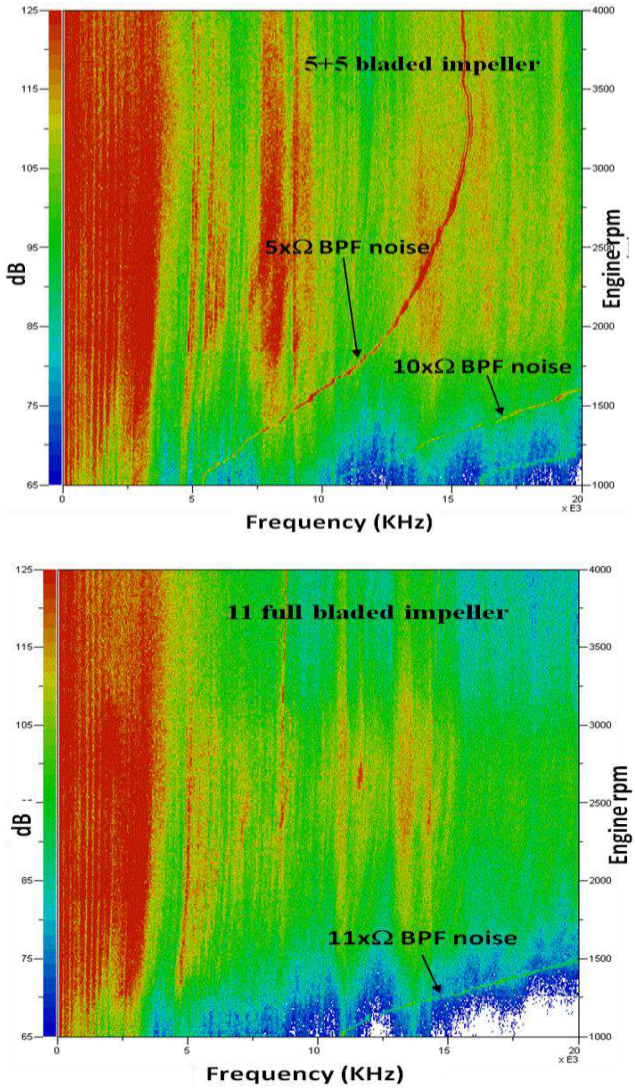

Figure 7 Measured on engine SPL level of BPF noise at exit of two turbocharger compressors. The large inducer blade number led to a significant reduction of BPF noise and a up-shift of its frequency

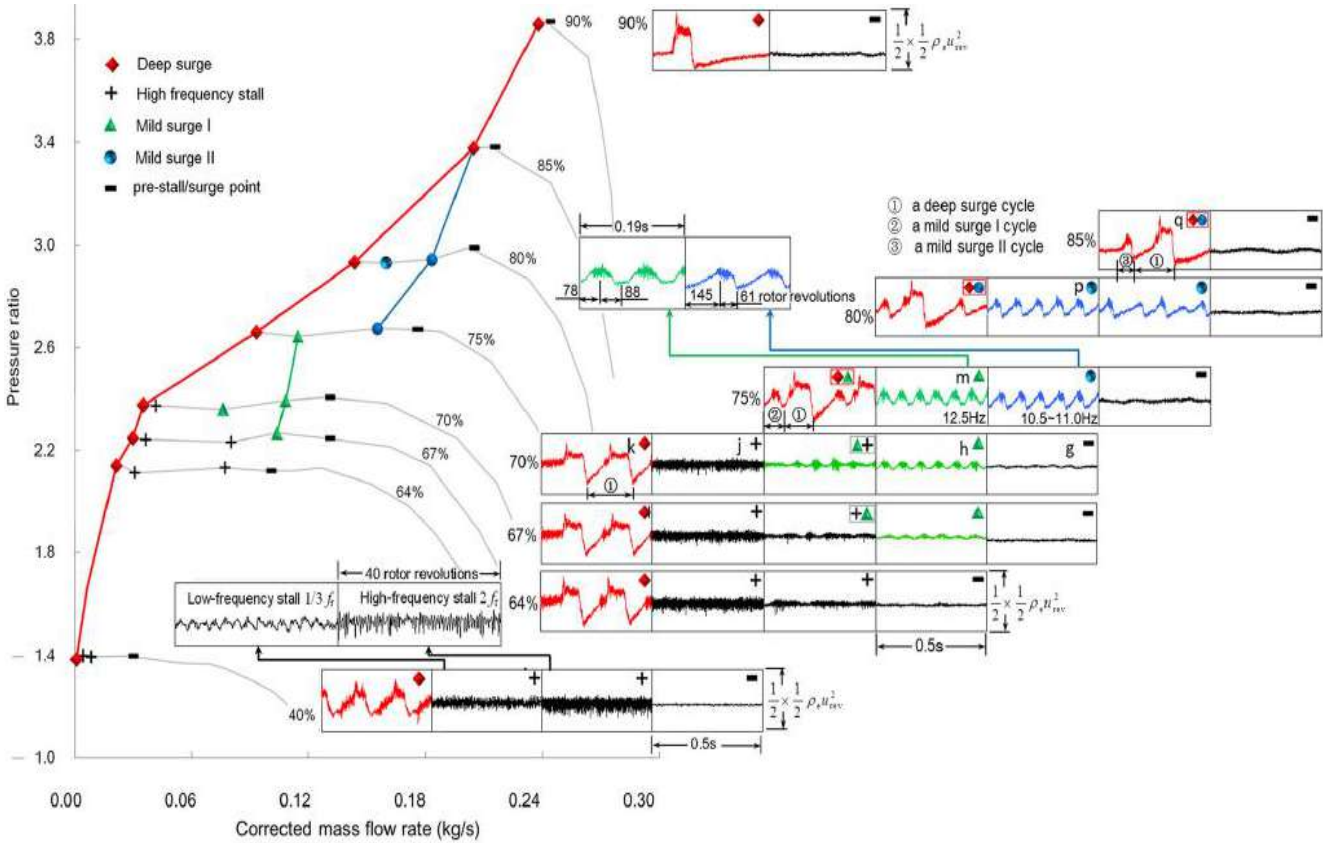

Fig. 8 Performance map of a turbocharger compressor with a vaneless diffuser, various instability regions are identified with associated casing static pressure signals taken in front of impeller LE. (22)

Deep surge (the red line and beyond in the figure) under which the compressor mass flow rate can become negative will not be discussed because this condition is to be avoided in compressor applications. To the right of the pre-stall/surge points, the compressor is stable as a system. These points are also the peak pressure ratio points: to their right, the speed-lines or pressure rise curves have negative slopes and are stable; to their left, the slope of the speed-lines becomes positive and the speed-lines become unstable, because if a small disturbance reduces compressor mass flow, the compressor pressure ratio will drop as well, and this drop diminishes the ability of the compressor to deliver mass downstream, and compressor mass flow will further decreases, resulting a positive feedback cycle of mass flow reduction. Mild surge is defined as the surge without global mass flow reversal. It is a resonance of compression system under instability. In compressor applications it is also better avoided but its mechanism is well understood, and the noise it created is of low frequencies as shown in **Figure 8**. So, we focus on other types of instability.

3.1Kelvin-Helmholtz instability related

Starting from the lowest speed-line in **Figure 8**, a noise of 2 x rotor rotating frequency was observed. This noise occurs before the more familiar rotating stall, and maybe caused by a Kelvin-Helmholtz instability recently reported by Bousquet et al (**23**). Kelvin-Helmholtz instability refers to an instability of shear layers. The large velocity gradient across a shear layer makes it unstable. In centrifugal impellers, increased incidence and loading near LE when compressor mass flow rate is reduced generate a LE tip leakage flow from blade p.s. to the s.s. This leakage flow is of high vorticity and moves with a different speed from those of surrounding fluids, forming a unstable shear layer, **Figure 9a**). Vortices are then produced by the shear layer, migrate downstream and breakup under increased back pressure, **Figure 9b**). Like vortices shedding, this process produces noise. In this compressor, CFD predicted a two-lobe (circumferential wave number m = 2) wave with a dominating frequency about 6 times of rotor rotating frequency, **Figure 9c)**.

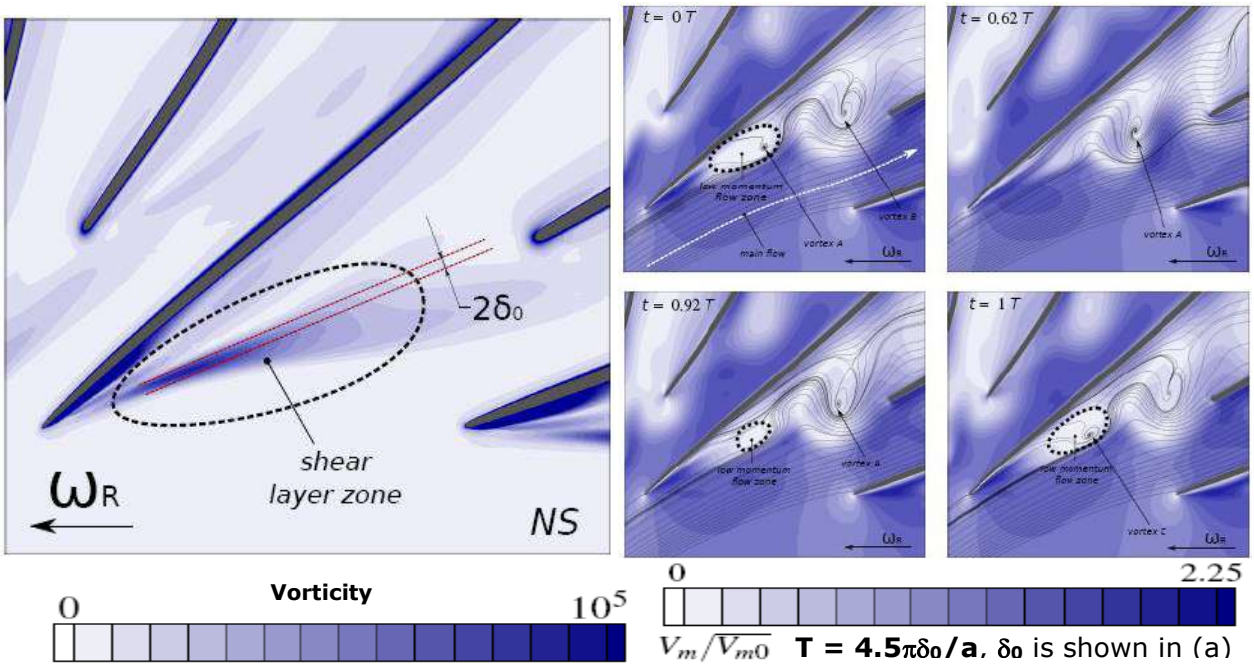

a) Time averaged magnitude of vorticity at 90% pan

b) Vortices (circled) formation, migration and breakup

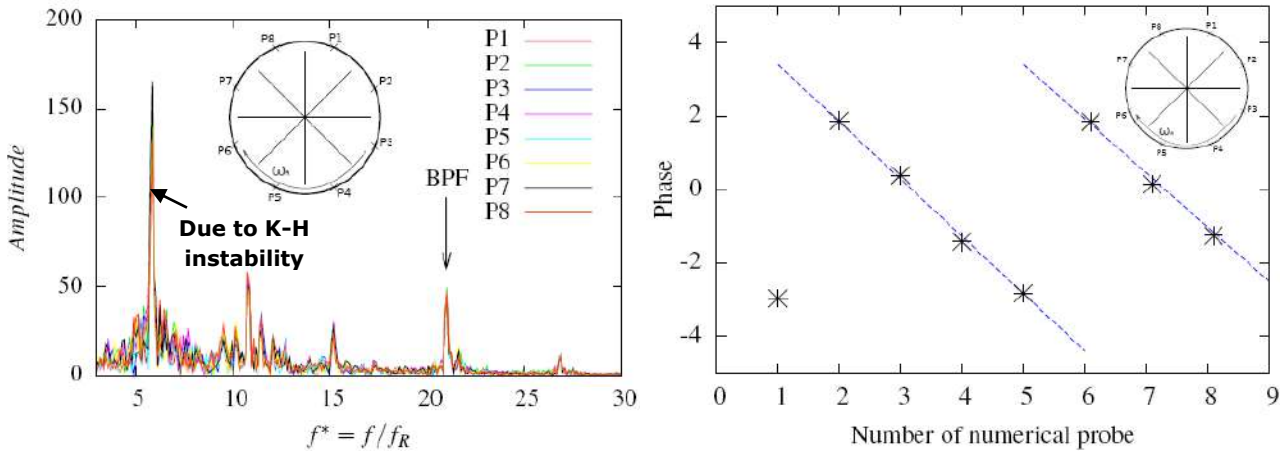

c) Pressure amplitude and phase at 8 numerical probes in 8 inducer channels. f_R is impeller rotating frequency

Fig. 9 URANS calculation of a centrifugal compressor operating near stall (NS) showing vortices generated by Kelvin-Helmholtz instability. The compressor has a 21 vanes diffuser (23).

3.2 Subsonic inducer rotating stall related

When the mass flow of the compressor in **Figure 8** further reduces, the TLV becomes stronger, larger and moves in more tangential direction due to increased LE blade loading and higher back pressure. **Figure 10** displays high speed camera images of TLV (LE tip leakage vortex) at two flow coefficients of a subsonic axial compressor. The smaller flow corresponds to pre-stall or near rotating stall condition. The vortex core enlargement, which signals vortex breakdown, and the vortex core movement towards tangential direction are visible under the reduced mass flow.

When the TLV eventually reaches or is near the LE of the adjacent blade, as sketched in **Figure 11**, the inducer loading of this blade is destroyed, compare **Figure 2(d)** and **Figure 2(g)**, causing this blade to stall and block the flow to its passage, and relieving the previously stalled blade. In travelling to the next blade, breakup of the TLV slows it down. And because of impeller rotation, the stalled blade channels or stall cells will rotate in the same direction of impeller in the absolute frame of reference, but in slower speeds. This generates a sub-synchronous noise in the rotating frequency of the stall cells which is a fraction of impeller rotating frequency. If number of stall cells is m, then a

noise with a frequency of m x rotating frequency of stall cells is also observed.

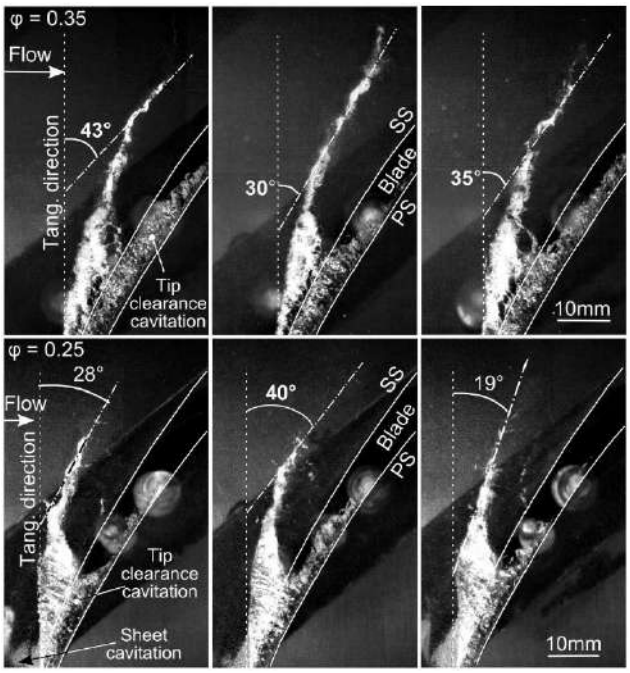

Fig. 10 High speed images of the cavitating tip leakage vortex of a subsonic axial compressor at two flow coefficients φ = 0.35 and 0.25 and three time instances. Compressor is near stall at the smaller φ value. (24)

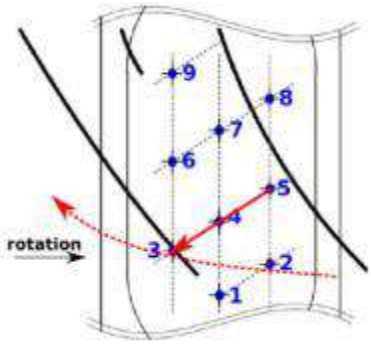

Fig. 11 Sketch of trajectories of TLV (broken red line) and overtip leakage flow (solid red line from 5 to 3) in rotating stall of a helicopter compressor, based on casing pressure signals from transducers 1 - 9. (25)

3.3 Diffuser stall related

While impeller inducer may stall, but it rarely triggers compressor surge directly. With the centrifugal force contribution to the overall pressure rise, centrifugal impeller's speed-lines do not have large positive slopes even in rotating stall conditions. A vaneless diffuser on the other hand always decelerates flow and is the most unstable component of the compression system. Its stall often triggers the stage stall and surge (**25-27**, see **Figure 15** as well). Because its inflow contains a large circumferential velocity component, the diffuser stall often occurs in the form of circumferential waves whose frequencies are linked to shaft speed. Vaneless diffuser can also have radial wave modes. Different number of stall cells may be formed at different operating conditions and with dissimilar geometries, resulting various noise frequencies being observed. **Figures 12** and **13** give examples of one- and two-cells rotating stalls of vaneless diffusers in two industrial compressors respectively. Note the strong disturbance caused by lobe passage in **Figure 13**. Three or four lobes vaneless diffuser rotating stalls were also often observed. **Figures 14** and **15** show an example.

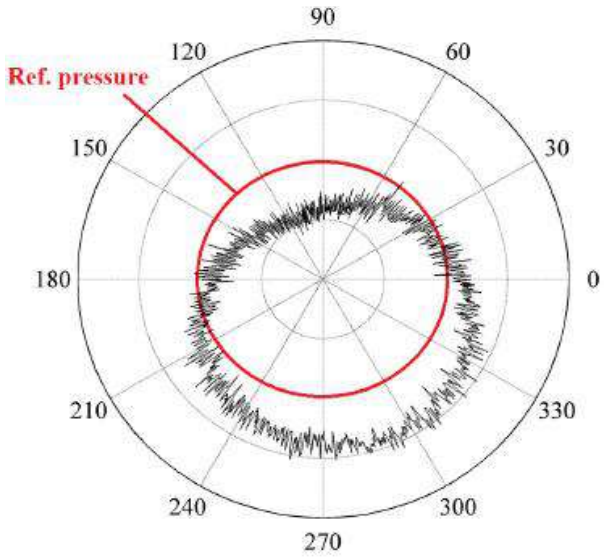

(a) Pressure at diffuser inlet

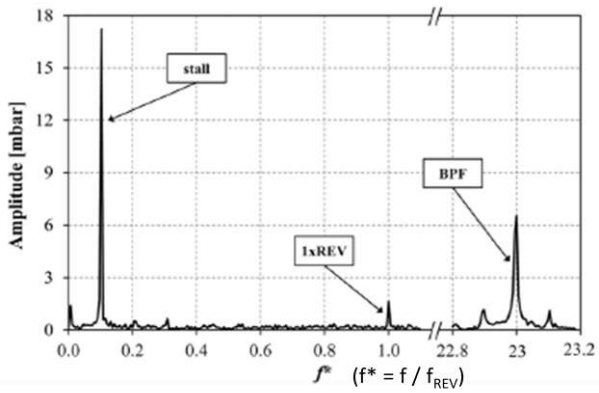

(b) FFT results of pressure signal

Fig. 12 Single lobed (m =1) stall of vaneless diffuser in an industrial centrifugal compressor. Blade Tip Mach no. = 0.85. (28)

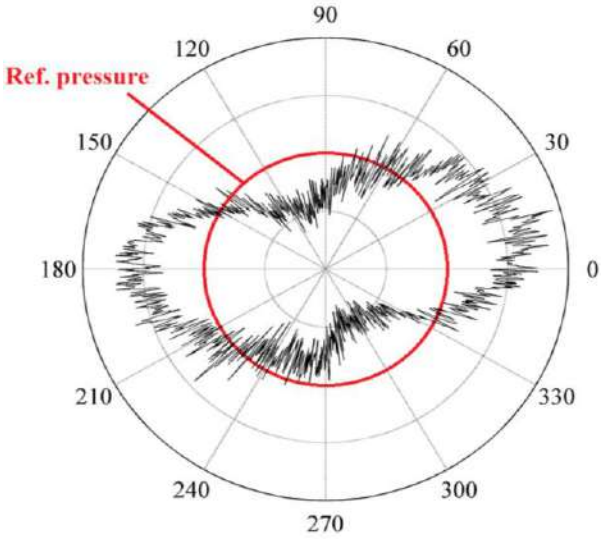

(a) Pressure at diffuser inlet

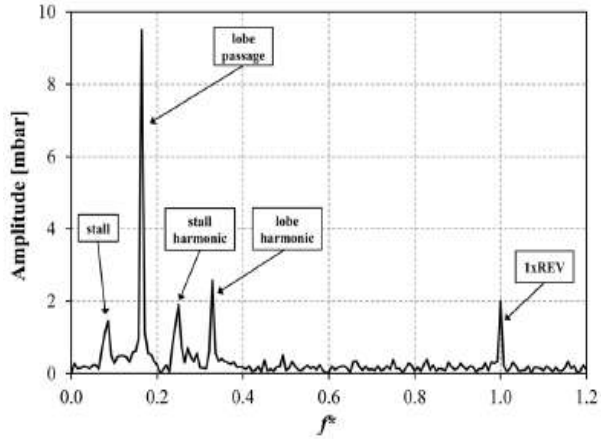

(b) FFT results of pressure signal

Fig. 13 Two lobed (m =2) stall of vaneless diffuser in an industrial centrifugal compressor. Blade Tip Mach no. = 0.5. (28)

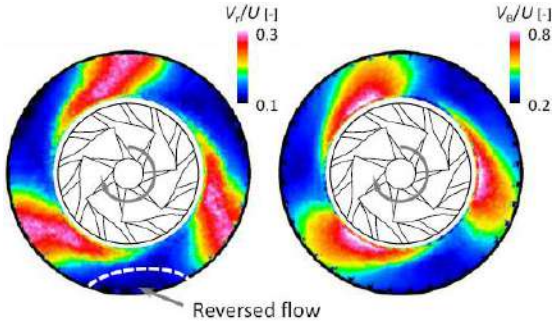

Fig. 14 Measured mid span flow velocities in vaneless diffuser at operating condition 5 (see Fig. 15) of a turbocharger compressor, showing three stalled regions or stall cells. (29)

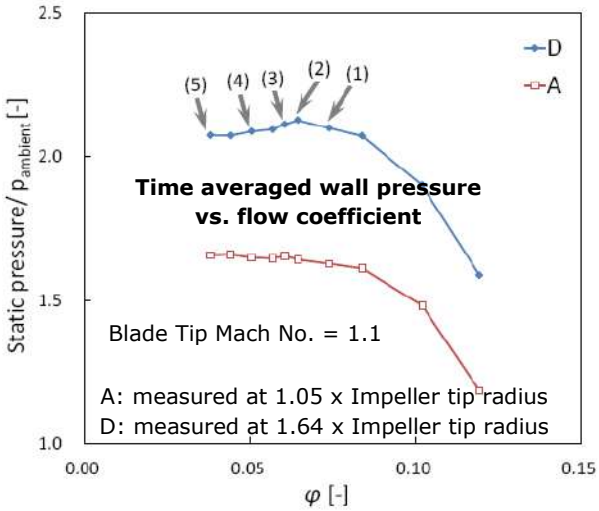

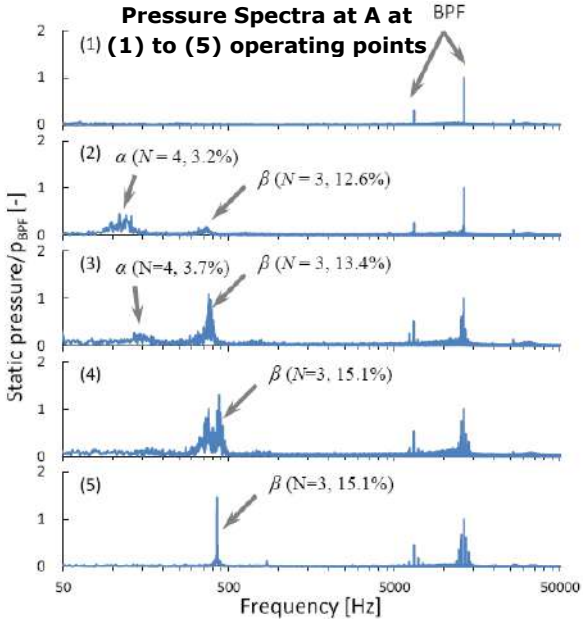

Numbers in the brackets indicate stall cell number and rotating speed of the cells divided by impeller speed

Fig. 15 Measured wall pressure spectra of a turbocharger compressor at five operating points at vaneless diffuser inlet (location A). (29)

Rotating speed of stall cells is typically < 50% of impeller rotating speed, but the lobe passage speed can be higher if lobe number is >1. If the stall pattern is nearly symmetric, only the lobe passage may be picked up by FFT and real stall cells rotation may become invisible. **Figure 16** presents such a case.

Chen and Sheng et al (**30-31**) proposed a rotating stall model for vaneless diffusers that allows estimation of the rotating speed and the number of the stall cells. They show that working with backsweep impellers vaneless diffusers can have two stalls at different flows, that is, in between the two stalls there is a stable region. This may explain why in **Figure 8** and in many

turbocharger compressor maps there exists a negative slope region to the left of the first positive slope region on the speed-lines.

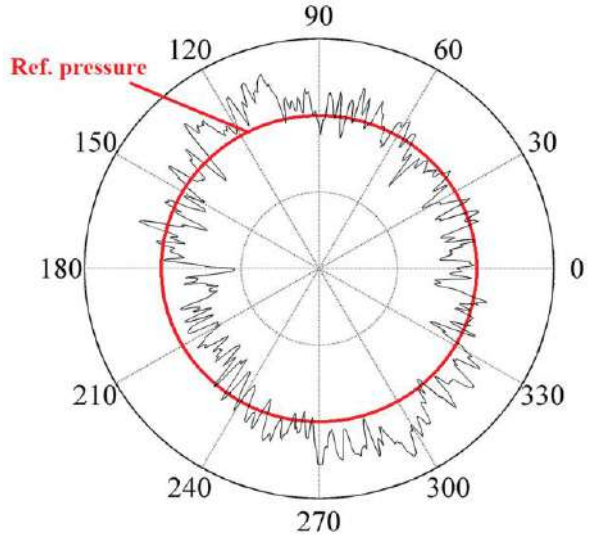

(a) Pressure at diffuser inlet

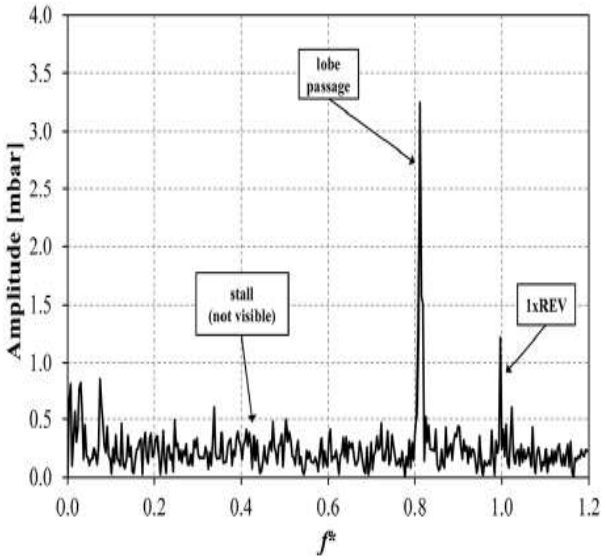

(b) FFT results of pressure signal

Fig. 16 nearly symmetric bi-lobed stall of vaneless diffuser in an industrial compressor. Blade Tip Mach no. = 0.65. (28)

3.4 Supersonic inducer stall related

At high compressor speeds, the stall mechanism of impeller inducers is slightly different from that at low compressor speeds, and shocks play an important role in inducer rotating stall. Near the stall, the LE shock is detached from the blade under increased back pressure, and the flow at the LE is subsonic, making the propagation of flow information in tangential direction and rotating stall possible. **Figure 17** depicts the inducer rotating stall inception of a compressor with vaneless diffuser. In the top picture of the figure, passage between blades 1 and 2 is stalled, the main passage shock on blade 1 s.s. causes TLV and overtip vortices to breakdown in shroud region, blocking the inflow to the passage. The blockage to the flow has reached the LE of blade 2 p.s., causing higher incidence to the blade 2. The larger incidence and the additional mass flow trying to get into the passage formed by blades 2 and 3 increase the Mach number on the s.s. of blade 2 thereby the shock strength in this passage, leading to severer flow breakdown and blockage in it (bottom picture of the figure) and relieving the previously stalled passage.

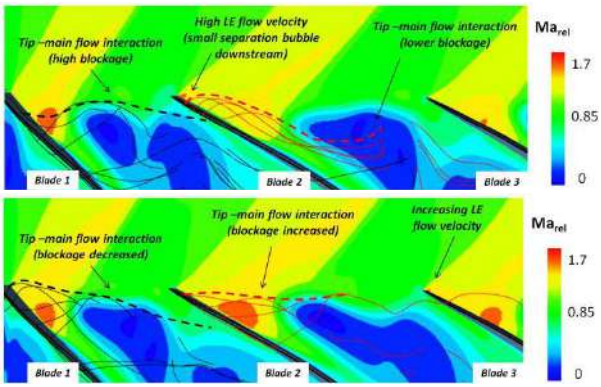

Fig. 17 URANS calculated relative Mach number at 92% span of a centrifugal compressor (9+9 bladed) at onset of inducer rotating stall at two time instances. Bottom picture was taken 1/8 rotor rev. after the top one. (32)

The pressure signal of **Figure 17** was analysed by FFT and shows distinct tonal feature peaked at about 5 times of rotor frequency, **Figure 18**. The rotating stall frequency itself is about 87% of the rotor frequency. The five times noise is likely caused by interaction between the blade passing and rotating instability, see next section.

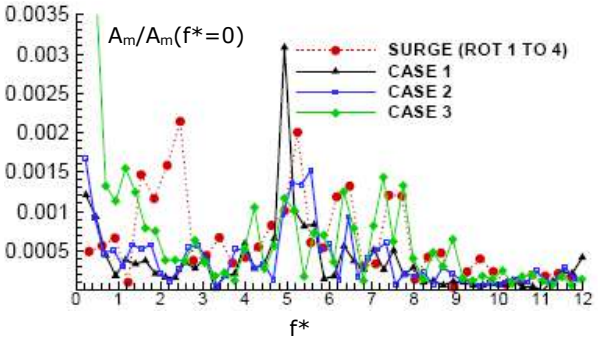

Fig. 18 Frequency Spectra of pressure signal by numerical probes located in vaneless diffuser at r/r_2 = 1.2 and 98% span on relative frame of reference with three different downstream throttle valve cases. Case 2 corresponds to Fig. 17. (32)

In addition to the noise generated by this rotating stall, the flow separation introduced by shocks is highly unsteady and causes the shocks foot at the boundary layer to oscillate. The oscillation generate a narrow band noise whose energy peaks at Strouhal number $Str = l_i \times f/V_\infty = 0.01 \sim 0.03$ (**33**), where f is the noise frequency, l_i is the distance shock foot oscillates and V_∞ the free stream velocity before the shock. For turbocharger compressors, the frequency of this noise is estimated in KHz to 10 KHz order. The strength of the noise is to be studied.

3.5 Scatter by rotor blades

The noise signals produced by compressor instability may get scattered by the rotation of the impeller blades when they propagate. The circumferential mode m at frequency f_m is scattered into modes $m_{R\&RI}$ at frequencies $f_{R\&RI}$,

$$\left.\begin{aligned} m_{R\&RI} &= i*B - j*m; \\ f_{R\&RI} &= i*B*\Omega_R - j*f_m; \\ i, j &= \ldots, -2, -1, 0, 1, 2, \ldots \end{aligned}\right\} \qquad (2)$$

where B is rotor blade no. and Ω_R the rotating frequency of the rotor. This scattering adds to the frequency spectra of compressors in stall and mild surge (during mild surge cycles, stalls happens intermittently, see for example (**22**)). **Figure 19** shows measured sound filed near the LE of an axial subsonic fan at the onset of rotating instability (RI). The fan rotor has 24 blades. The dominating modes of RI is 21 and 22. i = j = 1 in eq. (2) corresponds to BPF - RI in Figure 19.

3.6 Broad band noise

Broad band noise is associated with turbulence. vortices are generated when compressors work in stall and mild surge conditions. These large flow structures will breakdown under the adverse pressure gradient into smaller flow structures and eventually into turbulences as previously shown in **Figures 9** and **10**. **Figure 20** further demonstrates the mechanism of vortices breakdown where a simulated breaking down of a large vortex in compressor discharge section into smaller vortices and turbulences at instabilities of a turbocharger compressor is shown. Another source of broad band noise is the mixing of the incoming flow and the reversed flow at compressor inlet in stall and mild surge conditions (see for example (**35-36**)). Casing grooves, inlet vanes and inlet silencers, designed properly, can be and have been used to reduce the severity of the mixing and broad band noise.

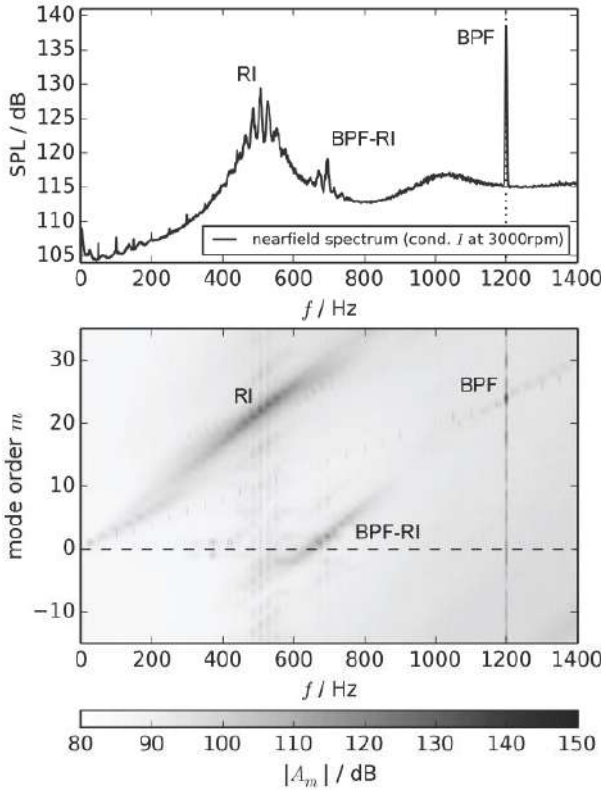

Fig. 19 Frequency spectrum (top) and decomposed circumferential mode amplitudes (bottom) of a subsonic axial fan showing scattering effect of rotor blades. (34)

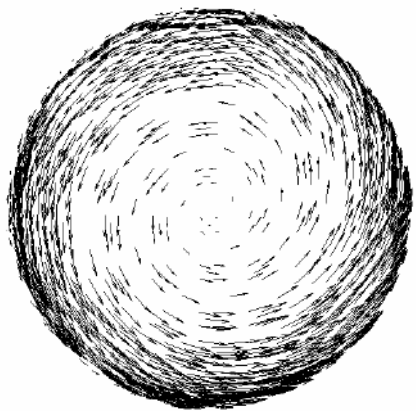

(a) Peak pressure ratio, single large vortex

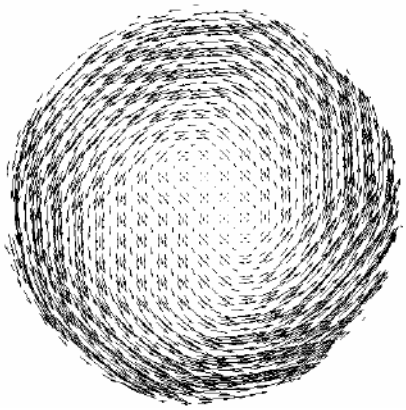

(b) Just in stall, two smaller vortices

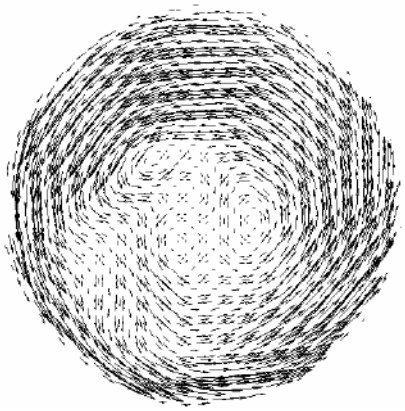

(c) Deep into stall, more small vortices

Fig. 20 Calculated flow structure at discharge section of a turbocharger compressor under various operating conditions. (26)

3.7 Reduce noise due to instability

The best method to reduce the noise produced by compressor instability is to make compressor stable. Delay diffuser stall or make the stall less severe can reduce the noise. One technique is to increase the turbulence of impeller exit flow so that the diffuser boundary layer is less likely to separate. One way of doing it is to use blunt impeller TE, instead of sharp one. The blunt TE sheds vortices downstream energising the diffuser flow. **Figure 21** shows the results. This method will slightly reduce compressor efficiency and as the figure indicates, the noise level at the choke end is slightly increased. Another technique to make the diffuser more stable is to reduce the diffusion in the diffuser, such as using a small diffuser exit-to-inlet diameter ratio. The loss of diffusion in the diffuser maybe compensated by using a larger volute, at least for low pressure ratio applications. Diffuser width and meridional contour can also be employed to control the diffuser instability. An examination of **Figures 12, 13** and **16** suggests that nearly symmetric stalls are better than asymmetric ones in noise aspect. How to link this observation to compressor design is to be explored.

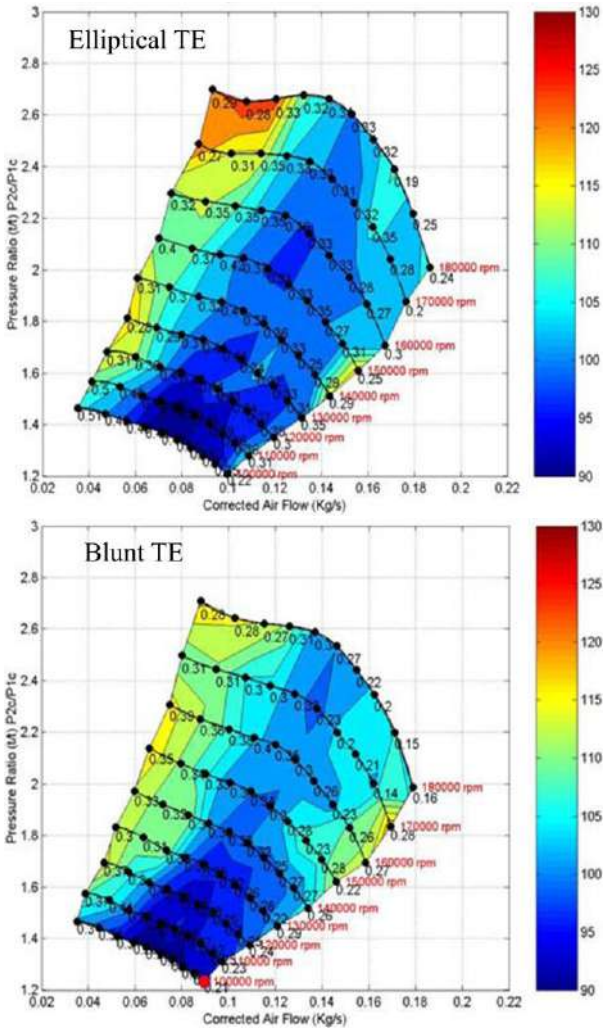

Fig. 21 Measured 500-4500Hz SPL (dB) maps of a turbocharger compressor with elliptical and blunt TEs.

Increase the flow area under the volute tongue can make flow more axisymmetric and improve compressor stability. Ported shroud is a very effective way to improve the stability of centrifugal compressors, it also reduces the strength of inducer passage shock (**37**). These two functions combined, ported shroud can greatly reduce noises due to flow instability and shocks. See **Figure 22**. Ported shroud may increases BPF noise in inlet pipe due to the enlarged casing front and interaction of port supporting ribs with BPF noise. It may also increase broad band noise with the flow separations inside the port. A silencer and other measures (**37**) can solve the problem.

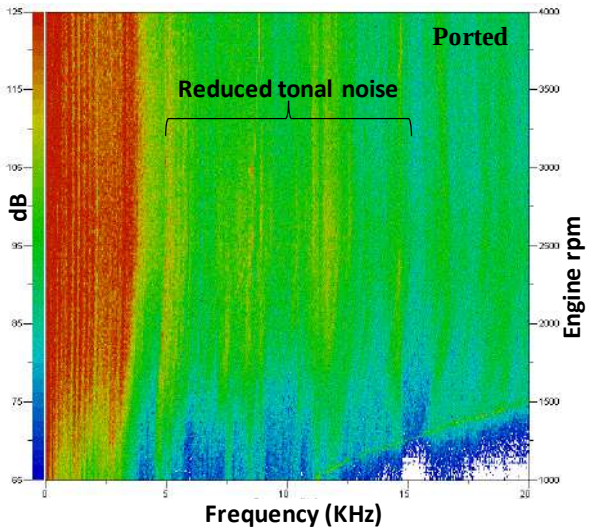

Fig. 22 Measured exhaust noise of a ported shroud compressor during engine transient. The compressor has 11 full blades. Non ported case is given in Fig. 7.

Impeller design has significant effects on compressor stability and associated noise. The aim is to have negative slopes for impeller speed-lines. High back-sweep angles and small shroud clearance should be used where possible. For high speed machines, the Mach number on blade s.s. should be restricted and the diffusion through the impeller controlled. 10~20° blade tip extension at shroud (mixed flow type tip) reduces the diffusion along the shroud and improves stability. **Figure 23** shows noise maps of three turbo-charger compressors. Design 1 is a radial type design and Designs 2 and 3 are of mixed flow tip. Both show improved noise characters to Design 1. Design 3 uses forward lean and full blades to further enhance stability, and displays the best noise character.

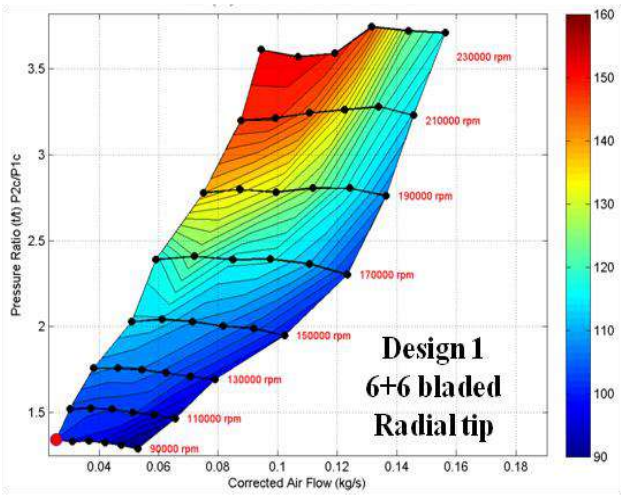

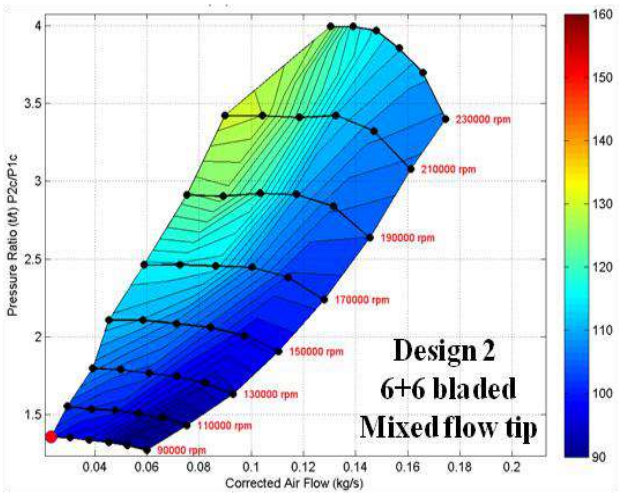

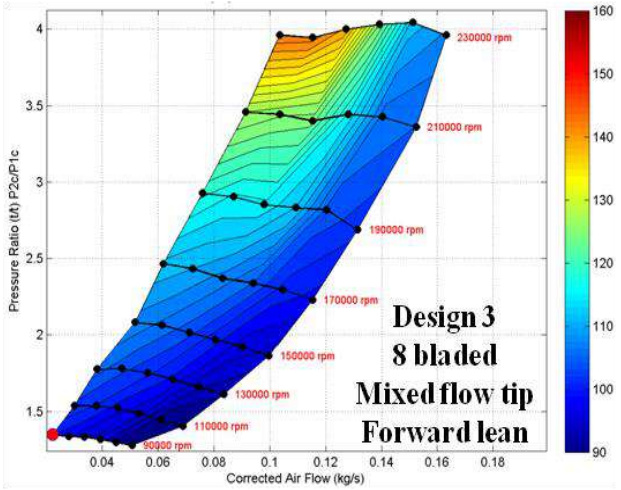

(a) Kreischen noise (2000-2800Hz)

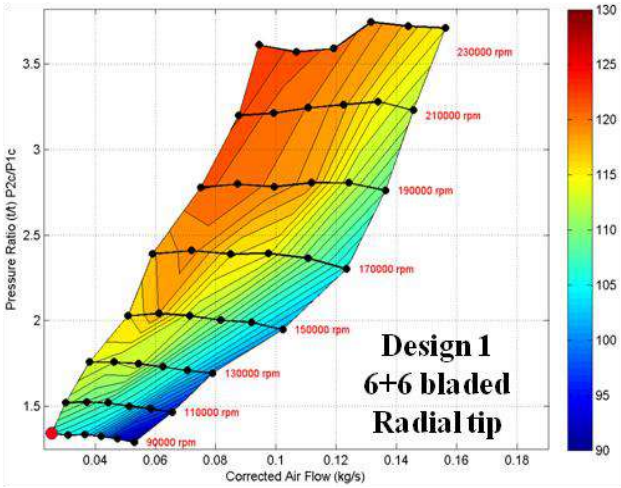

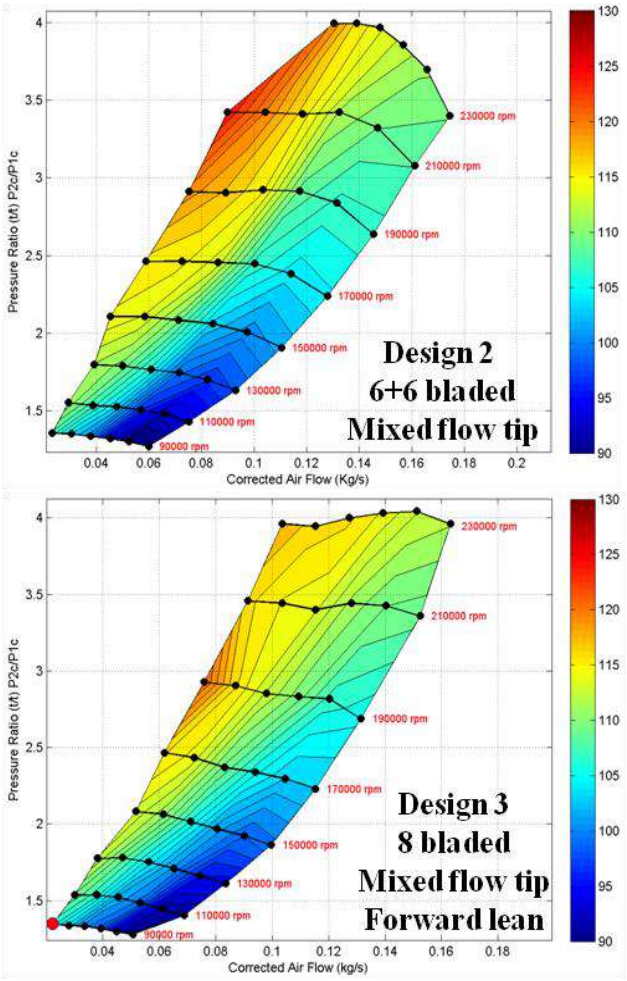

(b) Hiss (800-1800Hz) noise

Fig. 23 Measured noise (dB) maps of three small turbocharger compressors with different design philosophies

4. CONCLUSION

Factors affecting the BPF noise of compressors are discussed. Size, flow coefficient, speed, backsweep angle and blade number etc. are shown to be involved. Use of full bladed impellers is demonstrated to be an effective measure to reduce the BPF noise.

Both tonal and broad band noises by flow instabilities are examined for their aerodynamic sources. These include Kelvin-Helmholtz instability, vortex breaking down, subsonic and supersonic inducer rotating stalls, vaneless diffuser rotating stall, stall in volute discharge section, shocks boundary layer interaction and blade scattering effect. To reduce the noises, compressors should avoid positive slopes on their speed-lines. Various measures to improve compressor acoustic character, such as energising the diffuser flow, ported shroud, and impeller design philosophy such as mixed flow tip and forward lean etc, are illustrated.

5. ACKNOWLEGEMENTS

The author is grateful to his employer NLETT for allowing the publication of this paper.

6. REFERENCES

1. Feld H., Aschenbrenner A. and Girsberger R., (2001), Investigation of acoustic phenomena at the inlet and the outlet of a centrifugal compressor for pressure ratio 4.5. ASME Turbo Expo, 2001-GT-0314.
2. Clay D. and Moch S. W., (2002), Development of a new test facility for evaluation of turbocharger noise emissions. Proc. IMechE 7th Int. Conf. Turbochargers & Turbocharging, C602/032/2002. London.
3. Rämmal H. and Åbom M., (2007), Acoustic of turbochargers. SAE paper 2007-01-2205.
4. Brand J., Fallen M. and Kammer H., (2008), Future Technologies against turbocharger noise transferred to exhaust systems. SAE paper 2008-01-0891.
5. Schweizer B. and Sievert M., (2009), Oscillations of Automotive Turbocharger Turbine. J. Sound and Vibration, Vol. 321, pp. 955-975.
6. Tanna R. P. et al., (2010), Development of ported shroud compressor housing with reduced compressor blade pass source acoustic level. IMechE Ninth International Conference on Turbochargers and Turbocharging, C001/008/2010, pp115-124, London.
7. Lee Y., Lee D., So Y. and Chung D., (2011), Control of Airflow Noise From Diesel Engine Turbocharger. SAE paper 2011-01-0933.
8. Sheng X., (2012), 涡轮增压器噪声和振动．贯彻落实‘国四’排放标准技术交流会专题报告．(Turbocharger noises and vibrations), 17-18，May 2012，山东潍坊.
9. Kabral R., Rammal H. and Abom M., (2013), Acoustic methods for investigating turbocharger flow instability. SAE paper 2013-01-1879.
10. Karim A., Miazgowicz K., Lizotte B. and Zouani A., (2013), Computational aero-acoustics simulation of compressor whoosh noise in automotive turbochargers. SAE paper 2013-01-1880.
11. Dehner R. et al., (2013), Instability at the low-flow range of a turbocharger compressor. SAE paper 2013-01-1886.
12. Kuang X. et al., (2014), Surge noise identification and control of automotive turbochargers. SAE paper 2014-01-2053.
13. Åbom M. and Rämmal H., (2014), Turbocharger noise - Generation and Control. SAE paper 2014-36-0802.
14. Broatch A., Galindo J., Navarro R. and García-Tíscar J., (2014), Methodology for experimental validation of a CFD model for predicting noise

generation in centrifugal compressors. Intl. J. Heat and Fluid Flow, 50(2014) 134-144.
15. Biet C. and Baar R., (2015), Turbocharger Test Bench Extension for Acoustic Measurements at Cold Environment Conditions. SAE paper 2015-01-1672.
16. Gupta K, Vikram M. and Manta E., (2015), Study of Turbocharger Whistle Noise and Its Reduction Into Passenger Cabin. SAE paper 2015-26-0129.
17. Galindo J., Tiseira A., Navarro R. and Lprz M., (2015), Influence of tip clearance on flow behavior and noise generation of centrifugal compressors in near-surge conditions. Intl. J. Heat and Fluid Flow, 52(2015) 129-139.
18. Schleer M., Song S. and Abhari R., (2008), Clearance Effects on the Onset of Instability in a Centrifugal Compressor. ASME J. Turbo., July 2008, Vol. 130 / 031002-1.
19. Cumpsty N., (1989), Compressor Aerodynamics, Longman Group Ltd., Pearson Education Ltd, Harlow, Essex, U.K. ISBN 0-582-01364-X. (There is also a 2004 version with new Preface)
20. Bi Q., Chen H., Tong D. and Lu Y., (2016), A design method for globally curvature-smooth centrifugal compressor blades. ASME Turbo expo, GT2016-56416.
21. Roduner C., Kupferschmied P., Köppel P. and Gyarmathy G., (2000), On the Development and Application of the Fast-response Aerodynamic Probe System in Turbomachines—Part 2: Flow, Surge, and Stall in a Centrifugal Compressor. ASME J. Turbo., July 2000, Vol. 122, pp 517-526.
22. Zheng X. and Liu A., (2015), Phenomenon and mechanism of two-regime-surge in a centrifugal compressor, ASME J. Turbo., Vol. 137, 081007-1.
23. Bousquet Y., Carbonneau X. and Trebinjac I., (2015), Numerical investigation of Kelvin-Helmholtz instability in a centrifugal compressor operating near stall. ASME Turbo Expo, GT2015-42495.
24. Tan D. et al, (2014), Visualization and time resolved PIV measurements of the flow in the tip region of a subsonic compressor rotor. ASME TE, GT2014-27195.
25. Buffaz N. and Trébinjac I., (2012), Impact of tip clearance size and rotating speed on the surge onset in a high pressure centrifugal compressor. ASME Turbo Expo, GT2012-68427.
26. Chen H. et al. (2008), Numerical simulations of onset of volute stall inside a centrifugal compressor. ASME Turbo Expo, GT2008-50036.
27. Pullan G. et al, (2012), Origin and structure of spike-type rotating stall. ASME Turbo Expo, GT2012-68707.
28. Bianchini A. et al, (2014), Some guidelines for experimental characterisation of vaneless diffuser rotating stall in stages of industrial centrifugal compressors. ASME Turbo Expo, GT2014-26401.
29. Ohuchida S. and Tamaki H., (2013), Experimental study of rotating stall in vaneless diffuser of a centrifugal compressor. ASME Turbo Expo, GT2013-95468.
30. Chen H. et al, (2012), A 3-D compressible flow model for weak rotating waves in vaneless diffusers, Parts I & II. ASME J. Turbo. Vol. 134: 89–97 & 98-105.
31. Sheng F., Chen H., Zhu X. and Du Z. (2012), A three-dimensional compressible flow model for rotating waves in vaneless diffusers with unparallel walls. IMechE J. Mech. Eng. Sci., 226(9) 2230–2249.
32. Vagnoli, S. and Verstraete T., (2014), Numerical investigation of inlet distortion on the stall inception of a radial compressor. ASME Turbo Expo, GT2014-25516.
33. Clemens N. and Narayanaswamy V., (2014), Low-frequency unsteadiness of shock wave/turbulent boundary layer interaction. Annu. Rev. Fluid Mech. 2014, 46: 469-92.
34. Pardowitz B., Tapken U., Neuhaus L. and Enghardt L., (2014), Experiments on an axial fan stage: time resolved analysis of rotating instability modes. ASME Turbo Expo, GT2014-26323.
35. Tamaki H., (2015), Effect of Piping System on Testing of Centrifugal Compressors for Turbochargers. Turbocharging Seminar 2015, Sept. 2015, Tianjin, China.
36. Gancedo M., Guillou E. and Gutmark E., (2013), Experimental investigation of flow instability in a turbocharger ported shroud compressor. ASME Turbo Expo, GT2013-95134.
37. Chen H. and Lee V., (2013), Casing Treatment and Inlet Swirl of Centrifugal Compressors. ASME J. Turbo. July 2013, Vol. 135 / 041010.
38. Greitzer E., Tan C. and Graf M., (2004), Internal flow. Cambridge University Press. ISBN 0 521 34393 3.
39. LandauL. and Lifshitz E., (1987), Fluid Mechanics, 2nd Ed., Pergamon Press, Oxford, England.